

# Modelling the dusty universe II: The clustering of submillimetre-selected galaxies

C. Almeida<sup>1</sup>, C. M. Baugh<sup>2</sup>, C. G. Lacey<sup>2</sup>

<sup>1</sup>*Key Laboratory for Research in Galaxies and Cosmology, Shanghai Astronomical Observatory, Chinese Academy of Sciences, Nandan Road 80, Shanghai 200030, China.*

<sup>2</sup>*Institute for Computational Cosmology, Department of Physics, University of Durham, South Road, Durham, DH1 3LE, UK.*

16 October 2018

## ABSTRACT

We combine the GALFORM semi-analytical model of galaxy formation, which predicts the star formation and merger histories of galaxies, the GRASIL spectro-photometric code, which calculates the spectral energy distributions (SEDs) of galaxies self-consistently including reprocessing of radiation by dust, and artificial neural networks (ANN), to investigate the clustering properties of galaxies selected by their emission at submillimetre wavelengths (SMGs). We use the Millennium Simulation to predict the spatial and angular distribution of SMGs. At redshift  $z = 2$ , we find that these galaxies are strongly clustered, with a comoving correlation length of  $r_0 = 5.6 \pm 0.9 h^{-1} \text{Mpc}$  for galaxies with  $850 \mu\text{m}$  flux densities brighter than 5 mJy, in agreement with observations. We predict that at higher redshifts these galaxies trace denser and increasingly rarer regions of the universe. We present the predicted dependence of the clustering on luminosity, submillimetre colour, halo and total stellar masses. Interestingly, we predict tight relations between correlation length and halo and stellar masses, independent of sub-mm luminosity.

**Key words:** galaxies:high-redshift – galaxies:evolution – cosmology:large scale structure – submillimetre – methods:N-body simulations

## 1 INTRODUCTION

The discovery of a population of high-redshift galaxies selected by their emission at submillimetre wavelengths (submillimetre galaxies; SMGs) has opened a new window on star formation in the high redshift Universe (e.g. Smail et al. 1997; Hughes et al. 1997; Barger et al. 1998; Chapman et al. 2000; Blain et al. 2002). The commonly held belief is that the submillimetre flux from these galaxies is powered by prodigious star formation rates, which can reach up  $\sim 500 - 1000 M_{\odot} \text{ yr}^{-1}$  (Ivison et al. 2000; Smail et al. 2002; Chapman et al. 2005). The star formation is so intense that a substantial fraction of the mass of the present day descendants of SMGs, bright ellipticals, is thought to have been put in place during this phase (Borys et al. 2005; Michalowski et al. 2010). A further constraint on this picture would come from an estimate of the mass of the dark matter haloes which host SMGs. Measurements of the clustering of SMGs have so far proved challenging (Scott et al. 2002; Blain et al. 2004; Borys et al. 2005; Scott et al. 2006; Weiß et al. 2009). This situation has recently improved with the launch of the Herschel telescope and will continue to get better with the commissioning of the new SCUBA-2 camera on the James Clerk Maxwell Tele-

scope. In this paper we present predictions for the clustering of SMGs using a galaxy formation model set in the framework of the cold dark matter (CDM) cosmology.

The self-consistent modelling of SMGs presents a number of challenges. The sub-mm flux from a galaxy depends, often quite strongly, on a number of galaxy properties and parameters of the dust model, such as the star formation rate, the choice of the stellar initial mass function (IMF), the dust extinction (which is driven by the optical depth of the galaxy, which in turn depends on the metallicity of the cold gas and the size of the galaxy), the nature and composition of the dust grains and the thermal equilibrium temperature reached by the dust grains when heated by starlight. Granato et al. (2000) introduced a hybrid model which combined a calculation of the star formation histories of galaxies from the GALFORM semi-analytical galaxy formation model (Cole et al. 2000) with the spectro-photometric code GRASIL (Silva et al. 1998), which includes radiative transfer through a two-phase dust medium and a self-consistent prediction of dust temperatures. Using this model, a self-consistent calculation of the dust emission from galaxies can be made (Baugh et al. 2005; Lacey et al. 2008, 2010a).

Constructing a galaxy formation model which can re-

produce the observed number counts of SMGs is relatively straightforward. It is more challenging to go a step further and to match the number counts and the redshift distribution of SMGs at the same time. The task becomes much more difficult if, at the same time as matching the properties of high redshift galaxies, the model is also required to reproduce observations of the local galaxy population. Baugh et al. (2005) argued that it is only possible to achieve both of these goals by changing the slope of the IMF in episodes of star formation triggered by galaxy mergers. By adopting a top heavy IMF in starbursts, and by making the implied changes to the yield of metals and the fraction of gas recycled from dying stars, Baugh et al. were able to reproduce basic properties of SMGs. At the same time, the same model matches the observed luminosity function of Lyman-break galaxies from  $z = 3$  to  $z = 10$  (Lacey et al. 2010b), as well as being in good agreement with many observations of local galaxies. Nevertheless this model remains controversial and leads to conclusions which challenge the commonly accepted wisdom about SMGs. For example, González et al. (2010b) investigated the nature of SMGs in the Baugh et al. model and found that the SMG phase is not responsible for the formation of a significant amount of long lived stars. Here we present a further test of the model by presenting predictions for the clustering of SMGs.

To date, there are suggestions that SMGs are strongly clustered, with a correlation length that is substantially larger than that expected for the dark matter at the typical redshift of SMGs (e.g. Blain et al. 2004). However, the clustering measurements are currently noisy as a result of the small volumes surveyed, with this scatter being exacerbated by the strong clustering of the SMGs (Scott et al. 2002; 2006; Borys et al. 2004; Weiss et al 2009). There is only limited agreement between estimates of the angular clustering of SMGs, and poor agreement in turn between these measurements and the clustering inferred in three dimensions. The first results from the Herschel mission demonstrate the challenge of measuring the clustering of SMGs. Cooray et al. (2010) reported a detection of angular clustering in a sample of galaxies selected at  $250 \mu\text{m}$  from the Herschel HerMES survey, which they estimate to have a similar redshift distribution to the “classical” SMGs selected at  $850 \mu\text{m}$ , while Maddox et al. (2010), on the other hand, found no evidence for angular clustering for a galaxy sample selected in a similar way from the Herschel ATLAS survey. However, this situation is likely to improved rapidly as the Herschel surveys increase in size and are analysed in more detail. Also, the SCUBA-2 camera is currently being installed at the JCMT. The Cosmology Legacy survey using SCUBA-2 will produce a map of  $35 \text{ deg}^2$  at  $850 \mu\text{m}$ , substantially bigger than the SHADES Half-Degree Extragalactic Survey.

There are currently few predictions for the clustering of SMGs. van Kampen et al. (2005) compiled predictions for the angular clustering of SMGs from several groups. These calculations were phenomenological and did not attempt to predict the sub-mm flux from galaxies. The models were constrained by hand to match the SMG number counts. Here we make a direct prediction of which galaxies satisfy the selection criteria to appear in an SMG sample. Gas dynamic simulations are currently unable to provide meaningful predictions as the box sizes used are too small to predict clustering robustly beyond a scale on the order of a megaparsec.

Furthermore, in many cases these calculations stop at high redshift (again due to the small box size) and so cannot be tested against the local galaxy population. By using a semi-analytical approach, the computational resources can be devoted to modelling the evolution of the dark matter component, allowing us to use a representative cosmological volume.

In this paper we use the GALFORM+GRASIL model to populate the Millennium Simulation of the evolution of structure in a cold dark matter universe (Springel et al. 2005). This simulation occupies a volume of  $500 h^{-1}\text{Mpc}$  on a side and contains more than 20 million dark matter haloes at the present day. The CPU required by GRASIL makes it impractical to compute the spectral energy distribution for every galaxy directly in the Millennium Simulation. Instead, we apply a novel technique based on artificial neural networks (ANN) which we introduced in Paper I to populate the simulation with galaxies (Almeida et al. 2010).

The paper is organised as follows. In Section 2 we give a brief summary of the GALFORM+GRASIL model and explain how the artificial neural network is implemented. We show how well the model can predict the submillimetre luminosity of galaxies in Section 3. In Section 4 we present the predictions for the spatial and angular clustering of SMGs. The dependence of the clustering on selected galaxy properties is explored in Section 5. Finally, in Section 6, we present our conclusions.

## 2 MODEL

Here we give a brief summary of the semi-analytical galaxy formation model, GALFORM (§ 2.1), the spectro-photometric model used to compute galaxy SEDs, GRASIL (§ 2.2) and the artificial neural network (ANN) technique used to predict spectral properties for large samples of galaxies. Further details and tests of this approach can be found in Almeida et al. (2010).

### 2.1 The galaxy formation model: GALFORM

In this paper we use the GALFORM galaxy formation model to follow the fate of baryons in a  $\Lambda\text{CDM}$  universe. The general methodology behind semi-analytical modelling is explained in the review by Baugh (2006), and a more advanced overview of galaxy formation physics is given by Benson (2010). GALFORM was introduced by Cole et al. (2000). Descriptions of subsequent extensions to the model are given in Benson et al. (2003); Baugh et al. (2005) and Bower et al. (2006).

A summary of the model used in this paper, that of Baugh et al. (2005), can be found in Lacey et al. (2008, 2010a) and Almeida et al. (2010), where the processes modelled are described and the parameters used to specify the model are listed. Two changes from the original Baugh et al. set up are made as a result of the implementation of the model in the Millennium Simulation of Springel et al. (2005). Firstly, the cosmological parameters of the Millennium are different from those adopted in the Baugh et al. model.<sup>1</sup> We

<sup>1</sup> The Millennium Simulation adopts a flat  $\Lambda\text{CDM}$  cosmology

have found that by adjusting the baryon density parameter from the Baugh et al. value of  $\Omega_b = 0.045$  to  $\Omega_b = 0.033$  to give the same baryon fraction,  $\Omega_b/\Omega_m$ , as used in the original model, we obtain similar predictions for the galaxy luminosity function to those obtained in the original model. Secondly, we use the merger histories of the dark matter haloes extracted directly from the Millennium, constructed using the prescription described in Harker et al. (2006).

An important feature of the Baugh et al. model, particularly for the properties of galaxies selected by their dust emission, is the form of the stellar initial mass function (IMF) adopted in different modes of star formation. Bursts of star formation, which in this model are triggered by certain types of galaxy merger, are assumed to produce stars with a top-heavy IMF, where  $dN/d\ln m \propto m^{-x}$  and  $x = 0$ . Bursts are initiated by all major mergers (i.e. those in which the mass in cold gas and stars of the accreted galaxy account for 30% or more of the primary's mass) and by minor mergers in which the accreted satellite makes up at least 5% of the primary's mass and where the primary is gas rich (defined as 75% of the primary mass being in the form of cold gas; these figures are model parameters). Quiescent star formation in galactic disks is assumed to produce stars according to a solar neighbourhood IMF, the Kennicutt (1983) IMF, with  $x = 0.4$  for  $m < M_\odot$  and  $x = 1.5$  for  $m > M_\odot$ .

The adoption of a top-heavy IMF in starbursts is the key to reproducing the observed number counts and redshift distribution of faint sub-mm galaxies (Baugh et al. 2005; Swinbank et al. 2008). While this choice is controversial, a variety of observational evidence suggests that in some environments the IMF may have a higher proportion of high-mass stars than in the solar neighbourhood IMF (see the review by Elmegreen 2009). Moreover, the semi-analytical model is ideally placed to investigate the consequences for other predicted properties of assuming a top-heavy IMF in bursts. A number of predictions have been found to be in better agreement with observations following the use of different IMFs in the burst and quiescent modes of star formation, such as the metallicities of intra-cluster gas and of stars in early-type galaxies (Nagashima et al. 2005a,b). The precise form of the IMF is not important so long as a higher proportion of high mass stars are produced than would be the case with a solar neighbourhood IMF. Similar predictions would be obtained for an IMF with a standard slope which is truncated below a few solar masses. With a larger fraction of massive stars produced relative to the Kennicutt IMF, more energy is radiated in the UV and larger amounts of dust are produced due to the enhanced yield of metals.

In the next subsection we describe the GRASIL spectro-photometric code which generates a spectral energy distribution for each galaxy across a wide range of wavelengths. GALFORM itself makes an independent calculation of the spectral energy distribution (SED) of starlight, including a model for dust extinction which is described in Cole et al. (2000). This calculation gives similar results to those obtained with

with a present-day matter density  $\Omega_m = 0.25$ , a cosmological constant of  $\Omega_\Lambda = 0.75$ , a Hubble constant of  $h \equiv H_0/(100 \text{ km s}^{-1} \text{ Mpc}^{-1}) = 0.73$  and a perturbation amplitude given by the linear *rms* fluctuation in spheres of radius  $8h^{-1} \text{ Mpc}$  of  $\sigma_8 = 0.9$ . The original Baugh et al. model also assumes a flat  $\Lambda$ CDM cosmology but with  $\Omega_m = 0.3$ ,  $\Omega_\Lambda = 0.7$ ,  $h = 0.7$  and  $\sigma_8 = 0.93$ .

GRASIL at optical wavelengths. The GALFORM calculation of the V-band luminosity weighted age and optical depth are used as inputs to the ANN.

## 2.2 The spectro-photometric model: GRASIL

To accurately predict the SEDs of galaxies, from the far-UV to the radio, we use the spectro-photometric code GRASIL (Silva et al. 1998). This code computes the stellar emission, absorption and emission of radiation by dust, and radio emission powered by massive stars (Bressan et al. 2002). GRASIL carries out an accurate treatment of the extinction and reprocessing of starlight by dust.

The combination of GALFORM and GRASIL was described by Granato et al. (2000) and has been exploited in a series of papers (Baugh et al. 2005; Lacey et al. 2008, 2010a). The semi-analytical model calculates the star formation and metal enrichment history for each galaxy, including the contribution from starbursts. GALFORM also predicts the scale-lengths of the disk and bulge components of each galaxy, as described in Cole et al. (2000) and tested by Almeida et al. (2007) and González et al. (2009), and the cold gas mass (as compared against observations by Power et al. (2010) and Kim et al. (2010)). The dust is modelled as a two-phase medium, with a diffuse component and dense molecular clouds. The mass split between these components is a model parameter. In the Baugh et al. model, 25 per cent of the dust is assumed to be in the form of dense clouds. Stars form within molecular clouds and escape on a timescale  $t_{\text{esc}}$ , which is another model parameter; in Baugh et al. (2005), a value of  $t_{\text{esc}} = 1 \text{ Myr}$  is adopted in both quiescent and burst modes of star formation. The extinction of starlight by dust clouds depends on the star's age relative to the escape time. High mass stars, which typically dominate the emission in the UV, spend a significant fraction of their comparatively short lifetimes within molecular clouds. GRASIL calculates the radiative transfer of starlight through the dust and self-consistently solves for the temperature distribution of the dust grains at each point in the galaxy, based on the local radiation field. The temperature distribution of the grains is then used to calculate the dust emission. The composition and size of the dust grains are chosen to match the properties of the local ISM: a mixture of graphite and silicate grains, as well as polycyclic aromatic hydrocarbon (PAH) molecules. The effects of temperature fluctuations in very small grains and PAH molecules are taken into account. Emission from PAHs is calculated using the cross-sections of Li & Draine (2001). Radio emission from ionised HII regions and synchrotron radiation is included as in Bressan et al. (2002).

The GRASIL model has been calibrated against local observational data for normal and starburst galaxies (Bressan et al. 2002; Vega et al. 2005; Panuzzo et al. 2007; Schurer et al. 2009). A limitation of GRASIL is that it assumes axisymmetric distributions for the gas and dust in starburst galaxies. There is observational evidence of more complex geometries and extraplanar dust in some galaxies (see for example Engelbracht et al. 2006). This could be problematic if this dust absorbed and emitted a significant fraction of radiation. However, there is little observational evidence for this. Furthermore, observations of nearby starbursts reveal that most of the absorption and emission of radiation by dust takes place in a compact region of size  $\sim 1$

kpc or less. GRASIL has been shown to accurately predict the SEDs of both quiescent and starburst galaxies (Silva et al. 1998; Bressan et al. 2002).

### 2.3 The artificial neural network approach to predicting galaxy luminosities

The GRASIL code provides an accurate calculation of the absorption and reemission of radiation by dust, predicting the SED of a galaxy from the far-UV to radio. However, GRASIL is extremely CPU intensive, requiring several minutes to compute the SED for a single galaxy, which prohibits its direct application to extremely large numbers of galaxies. In Almeida et al. (2010) we introduced a new technique based on artificial neural networks (ANN) which can be used to rapidly predict SEDs using a small set of galaxy properties as input, once the ANN has been trained on a relatively small number ( $\sim 2000$ ) of galaxies with SEDs computed using GRASIL. We demonstrated that, in the majority of cases, this method can predict the luminosities of galaxies to within 10 per cent of the values computed directly using GRASIL. We employ the same approach in this paper. The general methodology behind the ANN is set out in detail in Almeida et al. (2010), so we give only a brief summary here. Silva et al. (2010) recently published a complementary approach in which the explicit calculation of emission by dust within GRASIL is replaced by an ANN.

Artificial neural networks are mathematical models designed to replicate the behaviour of the human brain. They are similar to their biological counterparts in the sense that ANNs consist of simple computational units, neurons, which are interconnected in a network. The neurons are usually organized in layers: an input layer, one or more hidden layers and an output layer. Each neuron has a weight associated with it. In this paper we will use a multilayer, feed-forward network. The ANN is trained using a sample of galaxies for which GRASIL has been run to compute spectra. During the training process, the neural network is presented with a set of inputs, comprised of selected galaxy properties, and associated outputs, in our case the luminosity at different wavelengths. The network weights are adjusted in order to reproduce, as closely as possible, the desired output from the given set of inputs. In summary: (i) we start with an untrained net (random weights); (ii) determine the output for a given input; (iii) compute the discrepancy or error between the predicted and the target output; and (iv) adjust the weights in order to reduce this error. To adjust the weights we use the resilient backpropagation learning algorithm (Riedmiller & Braun 1993).

As in Almeida et al. (2010), we use 12 galaxy properties predicted by GALFORM as input to the ANN: the total stellar mass, the stellar metallicity, the unextincted stellar bolometric luminosity, the disk and bulge half-mass radii and the circular velocities measured at these two radii, the V-band weighted age, the optical depth of dust extinction in the V-band, the metallicity of the cold gas, the mass of stars formed in the last burst and the time since the start of the last burst of star formation. Almeida et al. (2010) showed that the performance of the ANN is greatly improved if we predict only one output property, the luminosity in a single band-pass, instead of predicting the full SED of the galaxy (which typically covers 456 wavelength bins for a standard

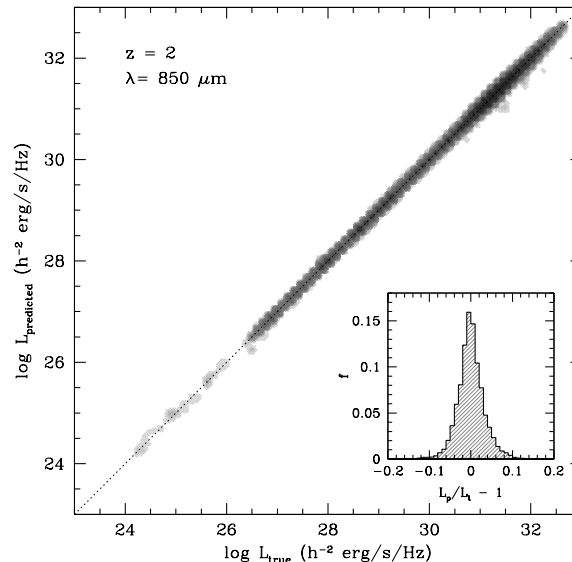


**Figure 1.** Comparison between the ANN predicted luminosity,  $L_{\text{predicted}}$ , and the true luminosity calculated using GRASIL,  $L_{\text{true}}$ , at  $850 \mu\text{m}$  in the observer frame for galaxies at  $z = 2$ . Note that a flux of 1 mJy at  $z = 2$  corresponds to a luminosity  $L_{\nu} = 4.75 \times 10^{31} h^{-2} \text{erg s}^{-1} \text{Hz}^{-1}$ . The shading shows the distribution of galaxies in the training sample. In the inset, we plot the error distribution of the predicted luminosities, as given by  $L_{\text{predicted}}/L_{\text{true}} - 1$ , normalized to unit area.

GRASIL SED). We then train the ANN separately for each band required. Here, we follow the same approach: we train two separate networks, one for each of the sub-mm wavelengths at which we want to predict luminosities ( $450 \mu\text{m}$  and  $850 \mu\text{m}$ ). The network configuration adopted has 12 neurons in the input layer, two hidden layers with 30 neurons each and one output neuron. We also found, in order to maximise the accuracy of the ANN predictions, that it was necessary to train the ANN at each redshift of interest, and to train separately for galaxies whose star formation is dominated by starbursts or quiescent star formation in disks.

### 2.4 The performance of the ANN at sub-mm wavelengths

We now demonstrate the how well the ANN performs when predicting galaxy luminosities in the sub-mm. Test at other wavelengths were presented in Almeida et al. (2010).

In Fig. 1 we plot the comparison between the observer frame luminosity in the SCUBA  $850 \mu\text{m}$  band predicted by the ANN for  $z = 2$  galaxies and the true values calculated directly using GRASIL. In this plot we include all galaxies regardless of their classification as quiescent or starburst galaxies. Fig. 1 shows that there is excellent agreement between the luminosities predicted by the ANN and the true values, with most of the predicted luminosities being within 10 per cent of the GRASIL result (inset). Some statistics quantifying the error distribution at different redshifts are summarized in Table 1, for galaxies brighter than 1 mJy in the corresponding band (either 450 or  $850 \mu\text{m}$ ). Here, the root mean squared logarithmic error,  $\varepsilon_L$ , is defined by:

Redshift	Sample	450 $\mu\text{m}$		850 $\mu\text{m}$	
		$\varepsilon_L$	$P_{ e <10\text{ per cent}}$	$\varepsilon_L$	$P_{ e <10\text{ per cent}}$
$z = 0.1$	Quiescent	0.04	97.1	0.04	98.6
	Burst	0.07	88.3	0.13	87.0
$z = 0.5$	Quiescent	0.04	96.9	0.04	98.5
	Burst	0.05	94.8	0.05	96.7
$z = 1$	Quiescent	0.06	94.9	0.04	97.0
	Burst	0.08	90.1	0.07	93.2
$z = 2$	Quiescent	0.04	97.2	0.04	97.5
	Burst	0.05	92.1	0.05	95.1
$z = 3$	Quiescent	0.05	96.0	0.03	97.8
	Burst	0.05	93.4	0.03	98.2
$z = 4$	Quiescent	0.04	97.0	0.03	98.5
	Burst	0.05	93.2	0.03	97.9

**Table 1.** Statistics of the error distribution associated with the ANN prediction of 450  $\mu\text{m}$  and 850  $\mu\text{m}$  observer-frame luminosities at selected redshifts. The statistics are computed using only galaxies with sub-mm fluxes brighter than 1 mJy in that band. Column 1 gives the redshift, column 2 specifies whether the galaxy sample is made up of galaxies forming stars quiescently or starbursts; columns 3 and 4 give  $\varepsilon_L$  (the root mean squared error defined by Eq. 1) and  $P_{|e|<10\text{ per cent}}$  (percentage of galaxies with predicted luminosities within 10% of the true value), respectively, for the 450  $\mu\text{m}$  predictions. For 850  $\mu\text{m}$  selected galaxies, the same information is shown in columns 5 and 6.

$$\varepsilon_L = \sqrt{1/n \sum^n [\ln(L_{\text{predicted}}/L_{\text{true}})]^2}, \quad (1)$$

where  $n$  is the number of galaxies considered. The quantity  $P_{|e|<10\text{ per cent}}$  is defined as the percentage of galaxies with predicted luminosities which lie within 10 per cent of the true values. For quiescent SMGs, we are able to reproduce the luminosities of more than 95 per cent of galaxies with an accuracy of 10 per cent or better, for the redshift range considered, at both 450  $\mu\text{m}$  and 850  $\mu\text{m}$ . As shown by Almeida et al. (2010), the performance of the ANN for burst galaxies is somewhat poorer, which is a consequence of the wide range of spectra seen in bursts and the difficulty the ANN experiences in reproducing this variety. Nonetheless the technique returns more than 90% of predicted sub-mm luminosities within 10 per cent of the true values. It should be noted that at  $z = 4$ , the highest redshift considered, the observer-frame 850  $\mu\text{m}$  luminosity probes the rest-frame 170  $\mu\text{m}$ , which is approaching the peak in the dust emission spectrum (typically around 100  $\mu\text{m}$ ).

One important feature of the error distribution is shown in the inset of Fig. 1. The distribution of luminosity errors predicted by the ANN appears to be Gaussian. Furthermore, we find that there is no correlation of the error with luminosity or other galaxy properties. This suggests that any sample of SMGs built using the ANN method will have errors which are decoupled from the structural and photometric properties of the galaxy sample.

### 3 CLUSTERING OF SUB-MM GALAXIES

The clustering of galaxies is an important constraint on the masses of their host dark matter halos, and hence on theoretical models of galaxy formation, as it depends upon how various physical processes vary with halo mass. In this section we present the model predictions for the clustering of galaxies selected by their flux at sub-mm wavelengths. In §3.1, we contrast the spatial distribution of galaxies with that of dark matter haloes. In §3.2, we define the two-point

spatial correlation function. We demonstrate that our clustering predictions are insensitive to errors in the galaxy luminosities predicted by the ANN in §3.3. We present the predictions for clustering in real space and redshift space in §3.4 and §3.5 respectively. The evolution of the correlation function is presented in §3.6 and the angular correlation function is shown in §3.7.

#### 3.1 The spatial distribution of SMGs

Before discussing the predictions for the two-point correlation function of SMGs, we first gain a visual impression of their spatial distribution. Fig. 2 shows dark matter haloes and sub-mm galaxies in a slice taken from the Millennium Simulation. The slice measures  $100 h^{-1}$  Mpc across and  $20 h^{-1}$  Mpc thick in comoving units. The upper panels show haloes and galaxies at  $z = 0.5$  and the lower panels show them at  $z = 2$ . Dark matter haloes are shown by the blue shading. The intensity of the shading is proportional to the total halo mass within each pixel. We show sub-mm galaxies selected at 450  $\mu\text{m}$  and 850  $\mu\text{m}$  with fluxes brighter than 1 mJy and 5 mJy. At a given flux limit, the 450  $\mu\text{m}$  sources are more numerous than the 850  $\mu\text{m}$  sources. The 850  $\mu\text{m}$  sources brighter than 1 mJy tend to trace out the more massive dark matter haloes and hence are expected to be biased tracers of the dark matter distribution. The full Millennium box ( $500 h^{-1}$  Mpc across) subtends an angle of 7.5 degrees at  $z = 2$ . To put this into context, we note that the SCUBA-2 Cosmology Legacy Survey (SCLS)<sup>2</sup> aims to map around  $35 \text{ deg}^2$  at 850  $\mu\text{m}$  in patches up to 3 deg across, and  $1.3 \text{ deg}^2$  at 450  $\mu\text{m}$  in regions up to 0.5 deg across. The nominal  $5\sigma$  flux limits will be 3.5 mJy at 850  $\mu\text{m}$  and 2.5 mJy at 450  $\mu\text{m}$ . However, source confusion may result in the flux limits for reliable source identification being somewhat brighter than this; using the standard 20 beams per source criterion for confusion (e.g. Lacey et al. 2008) together with the counts

<sup>2</sup> <http://www.jach.hawaii.edu/JCMT/surveys/Cosmology.html>

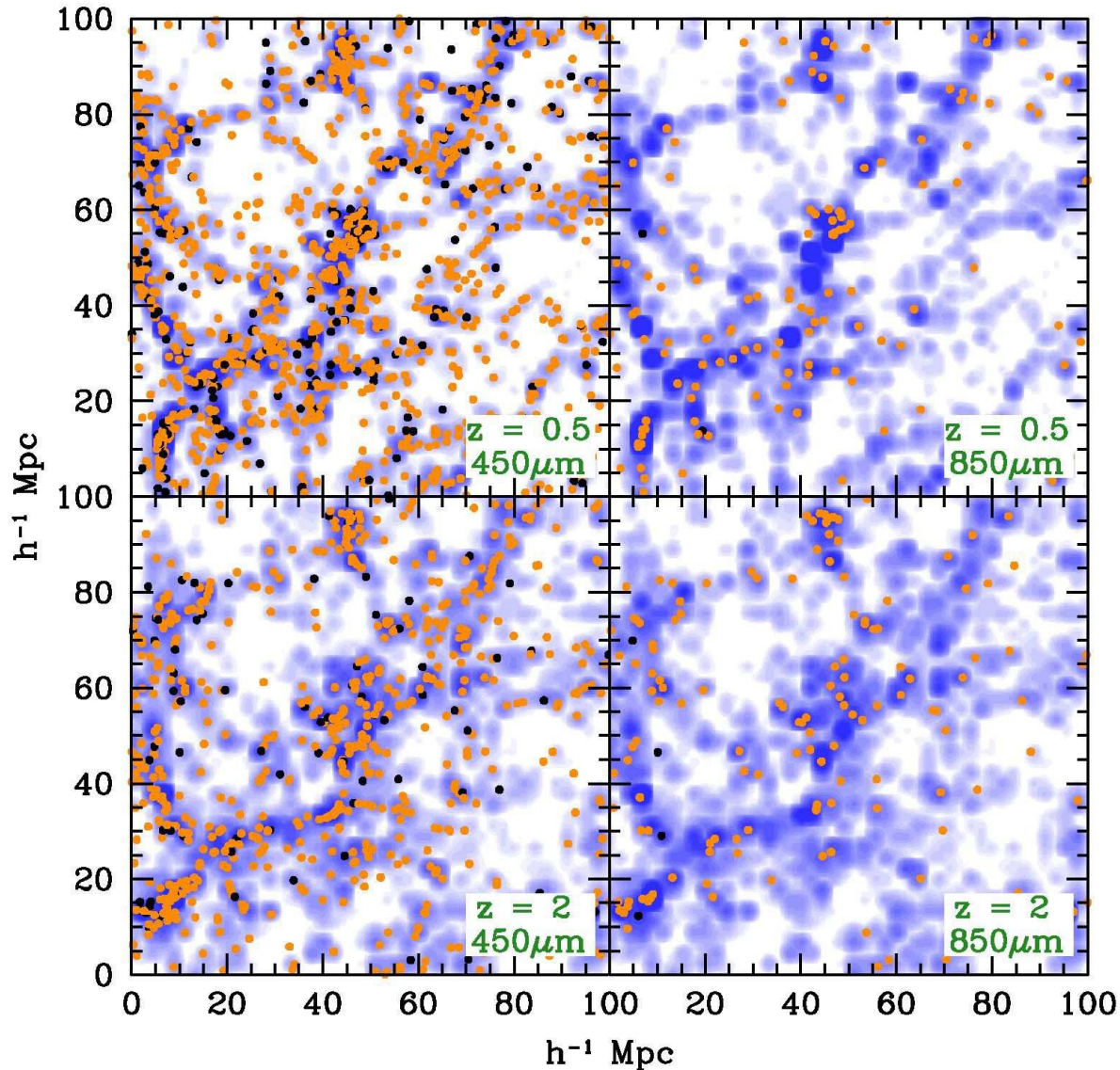


**Figure 2.** Image of the simulated spatial distribution of SMGs and dark matter haloes at  $z = 0.5$  (top panels) and  $z = 2$  (bottom panels). The panels display a slice  $100 h^{-1}$  Mpc wide with a depth of  $20 h^{-1}$  Mpc (in comoving coordinates). The width of this slice corresponds to angular scales of  $4.3^\circ$  and  $1.6^\circ$  at  $z = 0.5$  and  $z = 2$  respectively. The dark matter haloes are plotted in blue, with the darker shading corresponding to regions of higher projected halo mass density. Galaxies with  $S_{450\mu\text{m}}$  and  $S_{850\mu\text{m}} \geq 1$  mJy are represented by the orange dots. Brighter galaxies with  $S \geq 5$  mJy are shown by the black dots. The left hand panels show galaxies selected by their emission at  $450 \mu\text{m}$ , while the right hand side show galaxies selected by their emission at  $850 \mu\text{m}$ .

predicted by the model, we expect confusion to become important around  $3.0$  mJy at  $850 \mu\text{m}$  and  $5.3$  mJy at  $450 \mu\text{m}$ .

### 3.2 The two-point correlation function

To quantify the clustering of the galaxy distribution we use the two-point correlation function,  $\xi(r)$ , which gives the excess probability, compared with a random distribution, of finding two galaxies at a separation  $r$ :

$$\delta P(r) = \bar{n}^2 [1 + \xi(r)] \delta V_1 \delta V_2, \quad (2)$$

where  $\bar{n}$  is the mean space density of galaxies and the  $\delta V_i$  are elements of volume. If  $\xi(r) > 0$ , then galaxies are more

clustered than a random distribution. On the contrary, if galaxies have a tendency to avoid one other, then  $\xi(r) < 0$ .

The two-point correlation function of galaxies is shaped by two main factors, which play different roles on different scales. On large scales, the form of the correlation function is controlled by the clustering of galaxies in distinct dark matter haloes (referred to as the *two-halo term*), and the galaxy and dark matter correlation functions have similar shapes but differ in amplitude (for an illustration of this see Angulo et al. 2008). On smaller scales, up to the size of the typical haloes which host galaxies, the form of the correlation function is driven by the number and radial distribution of galaxies within the same dark matter halo, (called the *one-halo term*) (Benson et al. 2000; Seljak 2000).

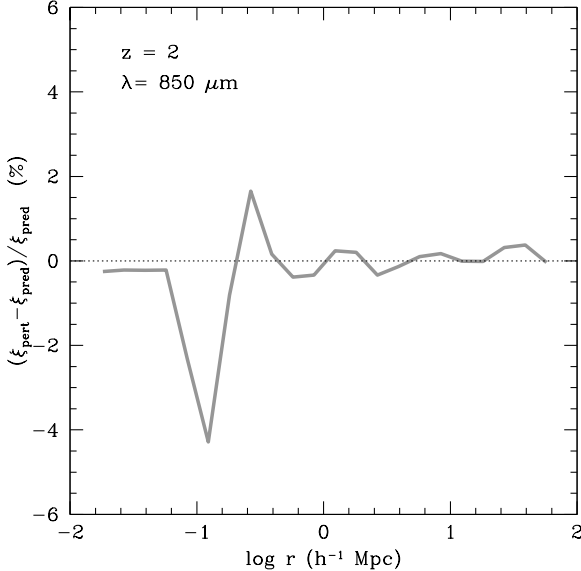


**Figure 3.** The impact of errors in the ANN predicted  $850\mu\text{m}$  luminosities on the form of the real-space two-point correlation function. The correlation function is measured for galaxies selected with fluxes brighter than  $1\text{ mJy}$  at  $z = 2$  ( $\xi_{\text{pred}}$ ). The galaxy fluxes are then perturbed using the error distribution of the ANN  $850\mu\text{m}$  luminosities and the correlation function is re-measured for the new sample of galaxies brighter than  $1\text{ mJy}$  ( $\xi_{\text{pert}}$ ). The plot shows the maximum deviation of  $\xi_{\text{pert}}$  from  $\xi_{\text{pred}}$  on constructing 20 different perturbed samples, expressed as a percentage. The spike around  $\log(r/h^{-1}\text{Mpc}) \approx -0.8$  is caused by noise due to the small number of galaxy pairs at that separation.

We calculate the two-point correlation function of sub-mm selected galaxies, using both real and redshift space coordinates. We measure the correlation function using the standard estimator (e.g. Peebles 1980):

$$\xi(r) = \frac{\langle DD(r) \rangle}{\frac{1}{2} N_{\text{gal}} \bar{n} \Delta V(r)} - 1, \quad (3)$$

where  $\langle DD(r) \rangle$  is the number of distinct galaxy pairs with separations between  $r$  and  $r + \Delta r$ ,  $N_{\text{gal}}$  is the total number of galaxies, and  $\bar{n}$  is the mean number density of galaxies.  $\Delta V(r)$  is the volume of a spherical shell of radius  $r$  and thickness  $\Delta r$ . We are able to compute the volume of this shell analytically since we are dealing with galaxy pairs within a periodic simulation volume. The clustering signal is generated in redshift space using the distant observer approximation, by electing one axis to be the line of sight direction, and adding the suitably scaled peculiar velocity of the galaxy along this axis to its comoving position.

### 3.3 The impact of luminosity errors on the predicted correlation function

We now look at the impact of errors on the ANN-predicted luminosities on the amplitude and shape of the two-point correlation function. First, the correlation function,  $\xi_{\text{pred}}(r)$ , is measured using the ANN-predicted observer-frame  $850\mu\text{m}$  luminosities for a sample brighter than some flux limit, in this case  $1\text{ mJy}$ . Next, these luminosities are

perturbed by drawing an offset from the distribution of errors expected for this band (see inset of Fig. 1 and Table 1). A new flux limited sample is constructed, which will contain some galaxies which were not included in the initial, unperturbed sample, because their fluxes have been boosted. Moreover some galaxies which made it into the original sample will no longer be included after their luminosities have been perturbed. We then repeat the measurement of the correlation function for this new sample, resulting in the estimate  $\xi_{\text{pert}}(r)$ . Comparing  $\xi_{\text{pert}}(r)$  with  $\xi_{\text{pred}}(r)$  provides an estimate of how  $\xi(r)$  is affected by the errors in the ANN-predicted luminosities. In Fig. 3 we plot the maximum deviation of the ratio  $\xi_{\text{pert}}(r)/\xi_{\text{pred}}(r)$  using 20 different  $\xi_{\text{pert}}(r)$  measurements for galaxies at  $z = 2$  (i.e. after perturbing the galaxy luminosities). This plot shows that  $\xi_{\text{pert}}(r)/\xi_{\text{pred}}(r)$  differs from unity by at most 4%, indicating that the clustering predictions are essentially unaffected by the errors in the ANN luminosities. At  $z = 0.1$ , where the performance of the ANN is poorer for galaxies undergoing a burst of star formation than it is at  $z = 2$ , the ratio  $\xi_{\text{pert}}(r)/\xi_{\text{pred}}(r)$  still deviates from unity by less than 10%.

### 3.4 The real space correlation function

In real space, the cartesian coordinates of the SMGs within the simulation box are used to calculate pair separations. Fig. 4 (top panel) shows the real space correlation function for sub-mm selected galaxies, for both  $\lambda = 850\mu\text{m}$  and  $\lambda = 450\mu\text{m}$ , at redshift  $z = 2$ . The transition between the one-halo term and two-halo term occurs around  $r \sim 0.6h^{-1}\text{Mpc}$ . In this plot we consider samples of galaxies selected to be brighter than  $1\text{ mJy}$  or  $5\text{ mJy}$  at both wavelengths. The black line shows the correlation function of the dark matter,  $\xi_{\text{DM}}$ , which was measured using a randomly chosen subset of  $10^6$  dark matter particles out of the ten billion particles in the Millennium Simulation.

As can be seen in Fig. 4, galaxies do not trace the mass distribution in the Universe, because the efficiency of galaxy formation depends on halo mass (e.g. Eke et al. 2004). The difference between the clustering of galaxies and the underlying dark matter is quantified in terms of the galaxy clustering bias,  $b$ :

$$b(r) = \left( \frac{\xi_{\text{gal}}(r)}{\xi_{\text{DM}}(r)} \right)^{1/2}. \quad (4)$$

Numerical simulations have demonstrated that the galaxy bias is a function of scale (Smith, Scoccimarro & Sheth 2007; Angulo et al 2008). This scale dependence weakens on large scales, and the galaxy bias is typically approximated as a constant. We plot the bias of SMGs in the lower panel of Fig. 4. The plot shows that at  $z = 2$  the bias factor is generally greater than unity, approaching a roughly constant value of  $b \approx 1.8$  for  $r \gtrsim 2h^{-1}\text{Mpc}$  for all of the samples shown. In the case of galaxies selected at  $450\mu\text{m}$ , there is a small but clear difference in the bias predicted for bright and faint samples, with the bright galaxies being the more strongly clustered. At  $850\mu\text{m}$  the distinction is less clear, due in part to the relatively low number density of galaxies in the bright sample, which results in a noisier prediction.

The effective bias parameter on large scales can also be estimated analytically (Mo & White 1996; Sheth, Mo & Tormen 2001), using the mass function

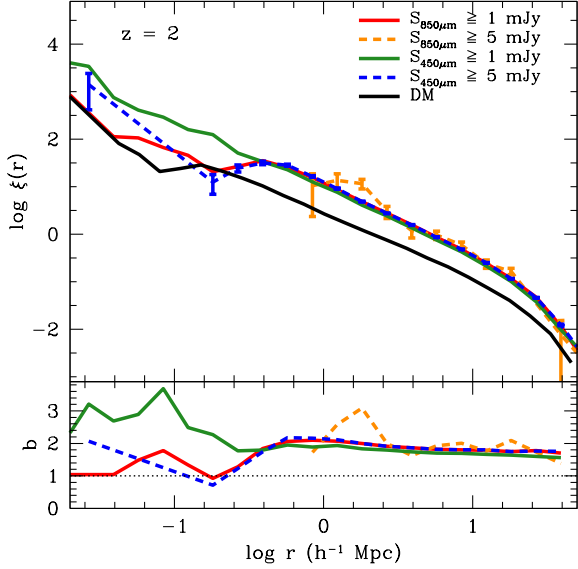


**Figure 4.** The real space two-point correlation function of sub-mm selected galaxies in comoving coordinates at  $z = 2$ . The blue and orange dashed lines show the predicted correlation functions for galaxies with fluxes brighter than 5 mJy at 450 and 850  $\mu\text{m}$  respectively, while the green and red lines show the corresponding results for a flux limit of 1 mJy. The black line shows the correlation function of dark matter. The errorbars show the  $1\sigma$  Poisson errors derived from the number of pairs in each bin of radial separation, and are only shown for those samples with the lowest total number of galaxies. In the bottom panel, we plot the galaxy bias,  $b(r)$ , as a function of scale for the four samples of sub-mm selected galaxies. This is obtained by taking the square root of the ratio of the galaxy correlation function to the measured dark matter correlation function.

of haloes which host sub-mm galaxies,  $N(z, M)$ , (i.e. the product of the space density or mass function of dark matter haloes and the halo occupation distribution of SMGs) and the bias factor as a function of the halo mass  $b(z, M)$  (e.g. Baugh et al. 1999):

$$b_{\text{eff}}(z) = \frac{\int_M N(z, M') b(z, M') d \ln M'}{\int_M N(z, M') d \ln M'} \quad (5)$$

The integrals are taken over the full range of halo masses, with  $N(z, M) = 0$  for haloes which do not host SMGs. To compute  $b(z, M)$  we use the prescription outlined by Sheth, Mo & Tormen (2001). For galaxies at  $z = 2$  with  $S_{850\mu\text{m}} \geq 5$  mJy, we find an effective bias of  $b_{\text{eff}} = 2.3$ , and  $b_{\text{eff}} = 2.1$  for sub-mm galaxies with  $S_{450\mu\text{m}} \geq 5$  mJy. These values are slightly larger than those estimated from the simulation using Eq. 4. In fact, similar differences between the analytical approach and simulations have been observed in other studies (see for example Gao et al. 2005; Angulo et al. 2009).

On small scales, Fig. 4 shows that the effective bias takes on a range of values. The clustering on these scales is driven by the typical number of galaxy pairs within a common halo. The faint sample of galaxies selected at 450  $\mu\text{m}$  displays the strongest clustering on small scales. This sample contains the largest number of pairs within common haloes. In the case of the brighter sample at 850  $\mu\text{m}$ , the low number

density of galaxies makes it difficult to measure the correlation function on small scales.

A convenient measure of the strength of clustering for different galaxy samples is provided by the correlation length  $r_0$ , which we can define in a robust way as the pair separation at which the correlation function becomes unity:

$$\xi(r_0) = 1. \quad (6)$$

Applying this definition to model galaxies selected at 850  $\mu\text{m}$ , we find  $r_0 = 5.6 \pm 0.9 h^{-1} \text{Mpc}$  for  $S_{850\mu\text{m}} \geq 5$  mJy, and  $r_0 = 5.38 \pm 0.02 h^{-1} \text{Mpc}$  for a fainter sample with  $S_{850\mu\text{m}} \geq 1$  mJy. We also find that 450  $\mu\text{m}$  selected galaxies are less clustered than 850  $\mu\text{m}$  selected galaxies at the same flux limit: we obtain  $r_0 = 5.38 \pm 0.02 h^{-1} \text{Mpc}$  and  $4.99 \pm 0.01 h^{-1} \text{Mpc}$  respectively for  $S_{450\mu\text{m}} \geq 5$  mJy and 1 mJy. SMGs with  $S_{450\mu\text{m}} \geq 5$  mJy display a similar two-point correlation function to that of  $S_{850\mu\text{m}} \geq 1$  mJy (as we will see later, this is mainly a consequence of the fact that the median  $S_{450\mu\text{m}}/S_{850\mu\text{m}}$  colour is approximately 3).

An alternative way to define the clustering length  $r_0$ , commonly used in observational studies, is to fit the correlation function with a power law:

$$\xi(r) = \left( \frac{r}{r_0} \right)^\gamma. \quad (7)$$

For optical galaxies at  $z \sim 0$ , this is found observationally to provide a good fit for  $0.1 < r < 10 h^{-1} \text{Mpc}$  with  $\gamma$  close to  $-1.8$  (e.g. Norberg et al. 2001; Zehavi et al. 2005). The two definitions of  $r_0$  (Eqs. 6 and 7) are obviously equivalent only if  $\xi(r)$  really is a power law. If  $\xi(r)$  actually has a more complicated dependence on  $r$ , then the value of  $r_0$  obtained by fitting a power law will depend on the range of  $r$  over which the fit is performed, and on the errors on the measurements at different  $r$ . If we fit  $\xi(r)$  for our model SMGs at  $z = 2$  with a power law over the range  $0.1 < r < 10 h^{-1} \text{Mpc}$ , we find  $\gamma = -1.8 \pm 0.2$  and a correlation length of  $r_0 = 6 \pm 1 h^{-1} \text{Mpc}$  for  $S_{850\mu\text{m}} \geq 5$  mJy, and  $\gamma = -1.61 \pm 0.01$  and  $r_0 = 5.21 \pm 0.05 h^{-1} \text{Mpc}$  for  $S_{850\mu\text{m}} \geq 1$  mJy. For galaxies with  $S_{450\mu\text{m}} \geq 5$  mJy, we find a slope similar to that of 850  $\mu\text{m}$  galaxies,  $\gamma = -1.62 \pm 0.01$ , and  $r_0 = 5.20 \pm 0.07 h^{-1} \text{Mpc}$ . The values of  $r_0$  obtained from the power law fit are thus close to the values obtained from the more general definition (Eq. 6) in this case. However, we will use Eq. 6 to define  $r_0$  unless stated otherwise.

Our predictions for the clustering of the brighter SMGs at 850  $\mu\text{m}$  are in reasonable agreement with the observational estimate by Blain et al. (2004) who, using a sample of 73 SMGs with  $S_{850\mu\text{m}} \geq 5$  mJy and spectroscopic redshifts at  $z \approx 2-3$ , inferred a correlation length of  $6.9 \pm 2.1 h^{-1} \text{Mpc}$  using a pair-counting approach rather than a direct measurement of  $\xi(r)$  (note this measurement is discussed further in §3.7).

We gain further insight into the clustering predicted by the model by plotting in Fig. 5 the mean number of sub-mm selected galaxies as a function of the halo mass, generally referred to as the halo occupation distribution or HOD (Benson et al. 2000; Cooray & Sheth 2002; Berlind et al. 2003). For completeness, we compute the median halo mass of our samples: for SMGs with  $S_{850\mu\text{m}} \geq 5$  mJy and 1 mJy, we find a median mass of  $1.4 \times 10^{12} h^{-1} M_\odot$  and  $9.3 \times 10^{11} h^{-1} M_\odot$ , respectively; whereas for  $S_{450\mu\text{m}} \geq 5$  mJy

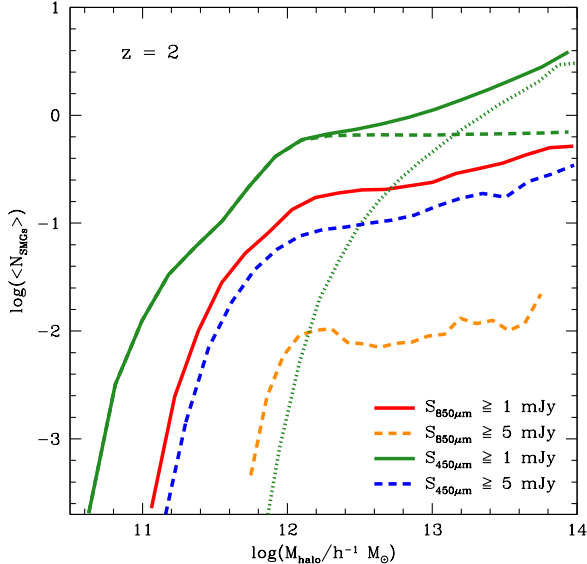


**Figure 5.** The predicted halo occupation distribution (HOD) of  $z = 2$  sub-mm selected galaxies. The dashed blue and orange lines show the HODs for galaxies brighter than 5 mJy at 450 and 850  $\mu\text{m}$ , while the green and red lines show the HODs for galaxies brighter than 1 mJy. The green dotted and dashed lines show the HOD of satellite and central galaxies with  $S_{450\mu\text{m}} \geq 1$  mJy, respectively.

and 1 mJy selected galaxies, we determine  $9.3 \times 10^{11} h^{-1} M_{\odot}$  and  $7.3 \times 10^{11} h^{-1} M_{\odot}$ . Fig. 5 shows that both our 850  $\mu\text{m}$  selected samples display a mean number of galaxies below unity over most of the range of halo masses. For example, in our model we find on average one  $S_{850\mu\text{m}} \geq 5$  mJy sub-mm galaxy for every  $\sim 100$  dark matter haloes of mass  $\sim 10^{13} h^{-1} M_{\odot}$ . This illustrates the need to consider a large number of halo merger histories in order to make robust predictions, a point we made previously for luminous red galaxies (Almeida et al. 2008). We also predict that these massive haloes, with  $M_{\text{halo}} \geq 10^{13} h^{-1} M_{\odot}$ , will accommodate more than one SMG with  $S_{450\mu\text{m}} \geq 1$  mJy (in our simulation, some haloes host more than 3 SMGs). If this was not the case, the two-point correlation function would tend to  $\xi \sim -1$  on scales smaller than the typical size of the host haloes (see Benson et al. 2000). For the case of  $S_{450\mu\text{m}} \geq 1$  mJy we plot the contributions of central and satellite galaxies to the HOD separately. The central galaxy HOD is seen to flatten above a certain mass, while the satellite HOD continues to rise and becomes a power law. It is interesting to note in this case that the HOD for central galaxies does not reach unity for any halo mass; around 70% of haloes with masses  $\geq 10^{12} h^{-1} M_{\odot}$  contain central galaxies brighter than 1 mJy at 450  $\mu\text{m}$ .

### 3.5 The redshift-space correlation function

Galaxy surveys usually use redshift to infer the radial distance to a galaxy, and the resulting measurement of clustering is said to be in redshift space. We therefore need to take into account the contribution of the peculiar velocity, induced by inhomogeneities in the galaxy's surround-

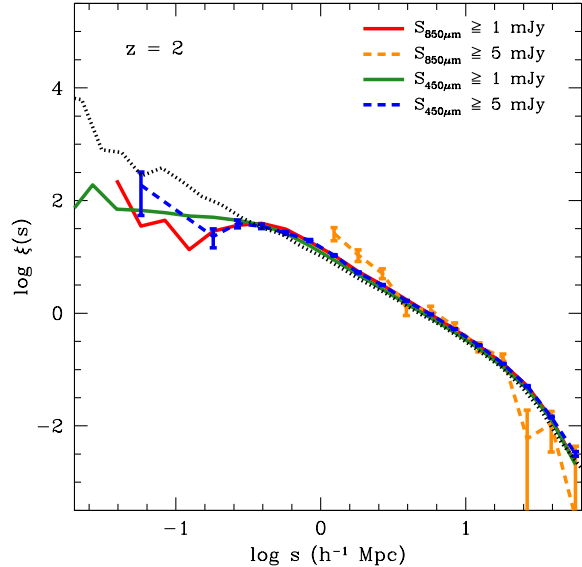


**Figure 6.** The redshift space two-point correlation function of sub-mm selected galaxies. The correlation function for 450  $\mu\text{m}$  and 850  $\mu\text{m}$  selected galaxies with flux densities brighter than 5 mJy, are represented by the dashed blue and orange lines, respectively, while solid green and red lines show galaxies with fluxes  $S_{450\mu\text{m}} \geq 1$  mJy and  $S_{850\mu\text{m}} \geq 1$  mJy. The errorbars show the  $1\sigma$  Poisson errors derived from the number of pairs. For comparison we plot the  $S_{450\mu\text{m}} \geq 1$  mJy real-space correlation function, using a dotted black line.

ing density field, to the position of a galaxy inferred from its redshift. To model redshift space, we perturb the position of the galaxy along one of the cartesian axes,  $x$ , by the peculiar velocity of the galaxy along this axis, scaled by the appropriate value of the Hubble parameter. This corresponds to the redshift position as viewed by a distant observer. The redshift space correlation function for galaxies selected by their sub-mm flux is plotted in Fig. 6. The impact of including the peculiar velocities on the correlation function (redshift space distortions) depends on scale. On intermediate and large scales, the bulk motions of galaxies towards large scale structures generate an amplification of the amplitude of the correlation function (see the comparison on large scales in Jennings et al. 2010). On small scales,  $r \lesssim 3 h^{-1} \text{Mpc}$ , the peculiar motions of galaxies within structures lead to a damping of the correlation function. In this case there is an apparent stretching of the structure in redshift space, which dilutes the number of SMGs pairs. As a consequence, if we calculate the correlation length in redshift space,  $s_0$ , following the definition given by Eq. 6, i.e.  $s_0$  is given by  $\xi(s_0) = 1$ , we obtain:  $s_0 = 6.4 \pm 0.5 h^{-1} \text{Mpc}$  for galaxies with  $S_{850\mu\text{m}} \geq 5$  mJy, and  $s_0 = 5.63 \pm 0.02 h^{-1} \text{Mpc}$  for fainter galaxies  $S_{850\mu\text{m}} \geq 1$  mJy, slightly larger than the real-space values given in §3.4.

### 3.6 The evolution of the correlation length

Having computed the spatial correlation functions of SMGs at  $z = 2$ , it is natural to study the evolution with redshift of the clustering properties of these galaxies. In Fig. 7 we plot

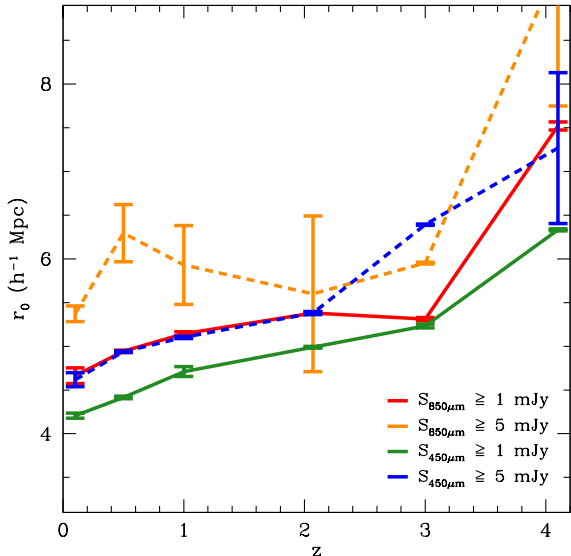


**Figure 7.** Evolution of the comoving correlation length with redshift for galaxies selected with  $S_{850\mu\text{m}} \geq 1$  mJy (red line),  $S_{850\mu\text{m}} \geq 5$  mJy (dashed orange line),  $S_{450\mu\text{m}} \geq 1$  mJy (solid green line), and  $S_{450\mu\text{m}} \geq 5$  mJy (dashed blue line).

the evolution of the comoving real-space correlation length,  $r_0$ , over the redshift interval  $z = 0 - 4$ , for galaxies selected to be brighter than either 1 mJy or 5 mJy at 450 or 850  $\mu\text{m}$ . Here we determine  $r_0$  by finding the scale at which  $\xi(r_0) = 1$ . The wavelengths quoted are in the observer’s frame, which means that, for example, at  $z = 4$   $\lambda = 850 \mu\text{m}$  corresponds to a rest-frame wavelength  $\lambda_{\text{rest}} \approx 170 \mu\text{m}$ . Over the typical redshifts at which SMGs are found (i.e. around  $z = 2$ ), Fig. 7 shows that the comoving correlation length is approximately constant. There is an increase in correlation length beyond  $z \sim 3$  and a decrease at  $z < 1$ , but very few galaxies appear in our samples at these redshifts. Fig. 7 indicates that the correlation length of galaxies selected at  $\lambda = 450 \mu\text{m}$  is usually smaller than of 850  $\mu\text{m}$  selected galaxies at the same flux limit. This is not surprising due to the fact that  $S_{450\mu\text{m}}/S_{850\mu\text{m}} \approx 3$  (see the colour distribution in Fig. 12), i.e. the same galaxy would appear about 3 times brighter at  $\lambda = 450 \mu\text{m}$  than at  $\lambda = 850 \mu\text{m}$ . This would then translate into a longer comoving correlation length (as we will see in Fig. 9).

### 3.7 Angular correlation function

The simplest measure of clustering in photometric galaxy surveys is the angular two-point correlation function,  $w(\theta)$ , which is a weighted projection of  $\xi(r)$  on the sky. The angular correlation function is used to measure clustering whenever redshift information is not available. In this case, the probability of finding two objects separated by angle  $\theta$  is similar to Eq. 2:

$$\delta P(\theta) = \bar{\eta}^2 [1 + w(\theta)] \delta\Omega_1 \delta\Omega_2, \quad (8)$$

where  $\bar{\eta}$  is the surface density of objects and  $\delta\Omega_i$  is an element of solid angle.

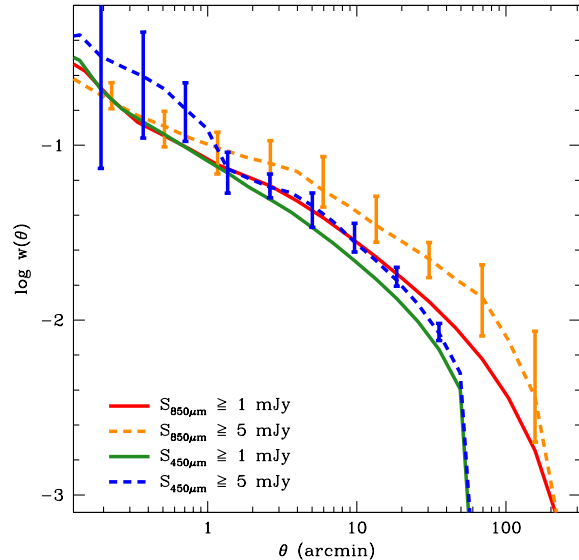


**Figure 8.** The two-point angular correlation function of sub-mm selected galaxies, computed directly from the spatial two-point correlation function. Galaxies selected at wavelengths of 450  $\mu\text{m}$  and 850  $\mu\text{m}$  with fluxes brighter than 5 mJy are shown by dashed blue and orange lines, while the green and red lines show galaxies with  $S_{450\mu\text{m}} \geq 1$  mJy and  $S_{850\mu\text{m}} \geq 1$  mJy respectively. The errorbars show the  $1\sigma$  Poisson errors derived from the number of pairs in each bin. These are computed for an area of  $1.3 \text{ deg}^2$  at 450  $\mu\text{m}$  and  $35 \text{ deg}^2$  at 850  $\mu\text{m}$ , to match upcoming surveys, as described in the text.

The galaxy formation predicts the spatial two-point correlation function,  $\xi(r)$ , and the redshift distribution of SMGs. From these predictions, it is straightforward to calculate the angular correlation function using Limber’s equation (Limber 1953). In a spatially flat universe, we have:

$$w(\theta) = 2 \frac{\int_0^\infty du \int_0^\infty x^4 \Psi^2(x) \xi(r, z) dx}{\left[ \int_0^\infty x^2 \Psi(x) dx \right]^2}, \quad (9)$$

where  $u$  is related to the comoving distance  $x$  by  $r^2 = u^2 + x^2 - 2xu \cos \theta$ . The selection function,  $\Psi(x)$ , gives the probability that a sub-mm galaxy at a distance  $x$  is detected in the survey, and is defined by:

$$\aleph = \int_0^\infty x^2 \Psi(x) dx = \frac{1}{\Omega_s} \int_0^\infty N(z) dz, \quad (10)$$

where  $\aleph$  is the surface density of galaxies,  $\Omega_s$  the solid angle covered by the survey, and  $N(z)$  gives the number of sources within  $z$  and  $z + dz$ .

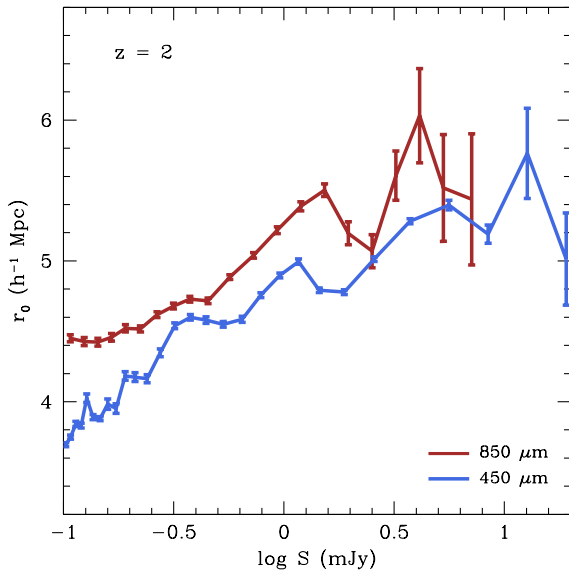
In Fig. 8 we plot the angular correlation function for 850  $\mu\text{m}$  and 450  $\mu\text{m}$  selected galaxies. We show predictions for galaxies brighter than 1 mJy and 5 mJy. We also show errorbars derived from the number of pairs in each bin in angular separation. These are computed for areas of  $1.3 \text{ deg}^2$  and  $35 \text{ deg}^2$  at 450  $\mu\text{m}$  and 850  $\mu\text{m}$  respectively, chosen to match the survey areas planned with SCUBA-2.

Fig. 8 shows that between 1 and 10 arcminutes,  $w(\theta)$  can be approximated by a power law:

$$w(\theta) = \left(\frac{\theta}{\theta_0}\right)^{1+\gamma}, \quad (11)$$

where  $\gamma$  is the same as in Eq. 7. The amplitude of clustering is characterised by  $\theta_0$ . This scale can vary from one sample to another because of differences in the intrinsic clustering and the redshift distribution of galaxies. Chance projections of galaxy pairs, as would occur more often in a catalogue which spanned a broad redshift interval, lead to a dilution of the clustering signal, which results in  $\theta_0$  decreasing with increasing survey depth (Peebles 1980). The predicted angular correlation function steepens slightly below  $\approx 1$  arcmin. Fig. 8 shows that bright SMGs are more clustered than faint SMGs. Fitting Eq. 11 to our samples over the range of angular scales  $1 < \theta < 10$  arcmin, with a fixed  $\gamma = -1.7$  (see previous section), we find a clustering scale of  $\theta_0(S_{850\mu\text{m}} \geq 5 \text{ mJy}) = 0.028 \pm 0.012$  arcmin. For galaxies selected by  $\lambda = 450 \mu\text{m}$  flux, we find  $\theta_0(S_{450\mu\text{m}} \geq 5 \text{ mJy}) = 0.022 \pm 0.007$  arcmin.

Observational estimates of the angular correlation function of SMGs suggest that these galaxies are strongly clustered. However, a consensus on the clustering amplitude of SMGs is yet to be reached. For example, using a small sample of SMGs observed with the SCUBA camera, Scott et al. (2002) found evidence of strong clustering on scales of 1 – 2 arcmin. In a follow-up study, Scott et al. (2006) re-reduced and combined different SCUBA surveys to measure the angular clustering and inferred a clustering scale  $\theta_0 \approx 0.6 - 0.8$  arcmin, depending on the precise choice of flux limit and signal-to-noise cut-off used to construct maps of SMGs. The challenge of measuring the clustering signal with such small samples is apparent from the size of the integral constraint correction typically applied. The integral constraint takes into account the fact that the true mean density of SMGs is not known when estimating fluctuations in the galaxy distribution. Instead, the density of the sample itself is used as a substitute for the true mean density. If the sample density is different from the true mean then the fluctuation level is misestimated, leading to a bias in  $w(\theta)$ . This effect is important for small samples and is even more severe if the galaxies are also strongly clustered. Scott et al. applied a correction of a factor of  $\approx 2$  to their measured clustering to account for the integral constraint. A subsequent measurement of clustering in a sample constructed with the LABOCA detector by Weiss et al. (2009) gives a correlation angle of  $\theta_0 = 0.23 \pm 0.12$  arcmin, which is substantially weaker than the Scott et al. result. The Weiss et al. estimate is still much larger than our model prediction, but differs from it by only  $1.8\sigma$ . Blain et al. (2004) made an indirect measurement of the spatial correlation function using radial pair counts of SMGs with spectroscopic redshifts, and obtained  $r_0 = 6.9 \pm 2.1 h^{-1}$  Mpc. For spatial clustering that is fixed in comoving coordinates, and using the observed redshift distribution of SMGs (Chapman et al. 2004), the Blain et al. result implies  $\theta_0 = 0.04 \pm 0.01$  arcmin, which is comparable to our model prediction. However, the method used by Blain et al. does not take into account fluctuations in the sample density, and should perhaps be viewed as providing a lower limit on the clustering strength.



**Figure 9.** The dependence of the comoving correlation length,  $r_0$ , on sub-mm flux for galaxies at  $z = 2$ . The predictions for SMGs selected by their emission at  $850 \mu\text{m}$  are shown by the red line, and those for  $450 \mu\text{m}$  selected sub-mm galaxies are plotted in blue. The flux plotted on the x-axis is correspondingly at either  $850$  or  $450 \mu\text{m}$ .

## 4 THE DEPENDENCE OF CLUSTERING STRENGTH ON GALAXY PROPERTIES

Here we consider the dependence of clustering strength on galaxy properties. We present the predictions for the two-point correlation function as a function of sub-mm flux, halo and stellar mass,  $S_{450\mu\text{m}}/S_{850\mu\text{m}}$  colour and the quiescent or starburst nature of galaxies at  $z = 2$ .

### 4.1 Dependence of clustering on sub-mm flux

In Fig. 9 we plot the comoving correlation length,  $r_0$  (computed using Eq. 6), as a function of sub-mm flux,  $S_\nu$ , for galaxies at  $z = 2$ . The plot shows that brighter galaxies have larger correlation lengths (see also Figs. 4 and 8). However, the dependence of clustering strength on luminosity is fairly weak, with a change of 50% in correlation length on changing flux by a factor of a hundred. This behaviour can be understood as a consequence of brighter galaxies being found predominately in more massive haloes, for which the bias is greater than unity and increases strongly with mass (Angulo et al. 2009). As already pointed out in relation to Fig. 4, for the same flux limit,  $450 \mu\text{m}$  selected galaxies are less clustered than their  $850 \mu\text{m}$  counterparts, with correlation lengths that are typically smaller by  $\Delta r_0 \approx 0.4 h^{-1}$  Mpc. This difference remains roughly constant throughout the range of sub-mm fluxes explored (in Fig. 13 we will see that this is a consequence of the fact that the median  $S_{450\mu\text{m}}/S_{850\mu\text{m}}$  colour is approximately  $\approx 3$ ).

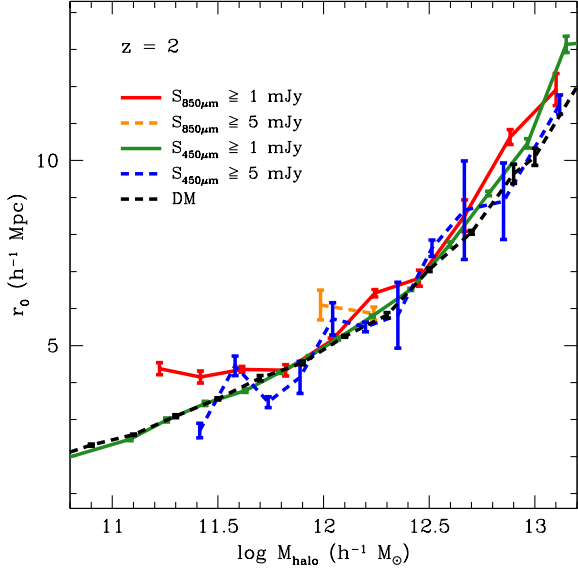


**Figure 10.** The dependence of the comoving correlation length,  $r_0$ , on host halo mass,  $M_{\text{halo}}$ , for galaxies at  $z = 2$  (for differential bins in halo mass). The red and green solid lines display the relation predicted for galaxies with  $S_{850\mu\text{m}} \geq 1$  mJy and  $S_{450\mu\text{m}} \geq 1$  mJy respectively. Brighter sub-mm galaxies, with fluxes above 5 mJy, are shown by the dashed orange ( $850\mu\text{m}$ ) and dashed blue ( $450\mu\text{m}$ ) lines. The dashed black line shows the dependence of correlation length on halo mass for all haloes (regardless of whether they host an SMG or not).

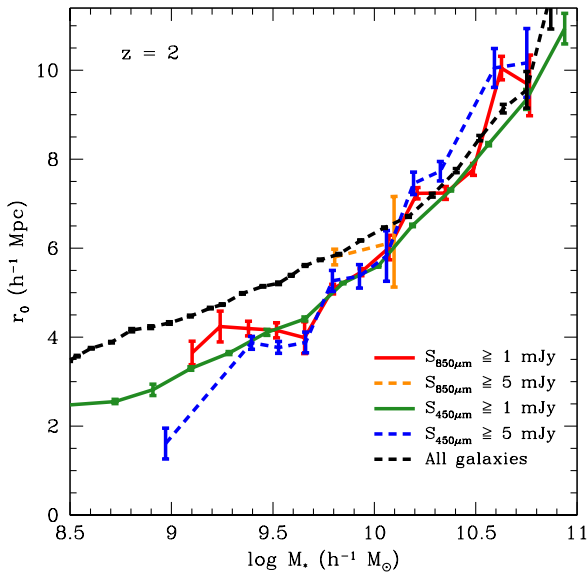


**Figure 11.** The dependence of the comoving correlation length,  $r_0$ , on total stellar mass,  $M_*$ , for galaxies at  $z = 2$ . The red and green solid lines display the predictions for galaxies with  $S_{850\mu\text{m}} \geq 1$  mJy and  $S_{450\mu\text{m}} \geq 1$  mJy, respectively. Brighter sub-mm galaxies, with fluxes brighter than 5 mJy, are shown by the dashed orange ( $850\mu\text{m}$ ) and dashed blue ( $450\mu\text{m}$ ) lines. The relation between  $r_0$  and stellar mass for all the galaxies in the simulation, regardless of their sub-mm flux, is shown by the dashed-black line.

## 4.2 Dependence of clustering strength on halo and stellar mass

Fig. 10 shows the dependence of  $r_0$  on the mass of the dark matter halo which hosts the SMG, for discrete bins in halo mass (the bin width is adjusted to contain a representative sample of galaxies). Remarkably, there is little difference between the clustering strength predicted for bright and faint samples of SMGs within a given bin of host halo mass. Moreover, the SMG clustering is essentially the same as that of all of the dark matter haloes in the mass bin, regardless of whether or not they contain an SMG. This means that the clustering strength of SMGs is driven purely by the mass of the host halo, and shows little or no dependence on a second property of the halo, such as its formation time or spin. One might have expected to see a dependence of the clustering strength at a given halo mass on SMG flux if this selection favoured host haloes which had, for example, formed more recently than the overall population at a given mass (see, e.g. Gao et al. 2005; Percival et al. 2003).

We now consider the dependence of the correlation length  $r_0$  on stellar mass,  $M_*$ , which we plot in Fig. 11. Following earlier plots, we display the relation for SMGs with fluxes brighter than 1 mJy at  $450\mu\text{m}$  and  $850\mu\text{m}$ , and for brighter samples with fluxes  $\geq 5$  mJy at both wavelengths. At  $z = 2$ , the median stellar masses of the model samples are  $M_* = 9.9 \times 10^9 h^{-1} M_\odot$  for galaxies with  $S_{850} \geq 1$  mJy, and  $M_* = 9.7 \times 10^9 h^{-1} M_\odot$  for those with  $S_{450} \geq 1$  mJy (see also González et al. 2010b). Comparisons with observational estimates of stellar masses are of limited use, as the results depend critically on the assumption made about the form of the stellar IMF (see Lacey et al. 2010a for an expanded discussion). For example, Hainline et al. (2010) estimated the stellar masses of  $\sim 70$  SMGs with  $S_{850\mu\text{m}} \approx 5$  mJy and found a median stellar mass of  $7 \times 10^{10} h^{-1} M_\odot$ , when using a Kroupa (2001) IMF. At the same flux limit, our model predicts a median stellar mass of  $2 \times 10^{10} h^{-1} M_\odot$ .

There is a tight, monotonic correlation between the comoving correlation length,  $r_0$ , and stellar mass,  $M_*$  (Fig. 11). Massive galaxies are more strongly clustered than galaxies with lower stellar masses, implying that more massive galaxies tend to be hosted by more massive haloes. Interestingly, all of our samples show a similar correlation length for a given total stellar mass, i.e. the relation between correlation length and total stellar mass does not depend on the sub-mm luminosity of the galaxy. We find that the correlation length  $r_0$  varies roughly linearly with  $\log M_*$  in the range  $\log M_* \approx [9.5, 10.5] h^{-1} M_\odot$ . Another important aspect is the fact that SMGs have, typically, weaker clustering than other galaxies of the same stellar mass. This is particularly evident for stellar masses below  $10^{10} h^{-1} M_\odot$ . The phenomenon is essentially due to the combination of two factors. Firstly, there is a difference in the host halo masses for satellite and central galaxies of the same stellar mass: at a given stellar mass, satellite galaxies inhabit haloes which are roughly ten times more massive than central galaxies. Secondly, SMGs galaxies with stellar masses lower than  $10^{10} h^{-1} M_\odot$  are mainly central galaxies, whereas the fraction of satellite galaxies for the full galaxy population is approximately 30 per cent. Submillimetre galaxies with stellar masses  $M_* \geq 10^{10} h^{-1} M_\odot$  display a similar fraction of satellite galaxies to that in the

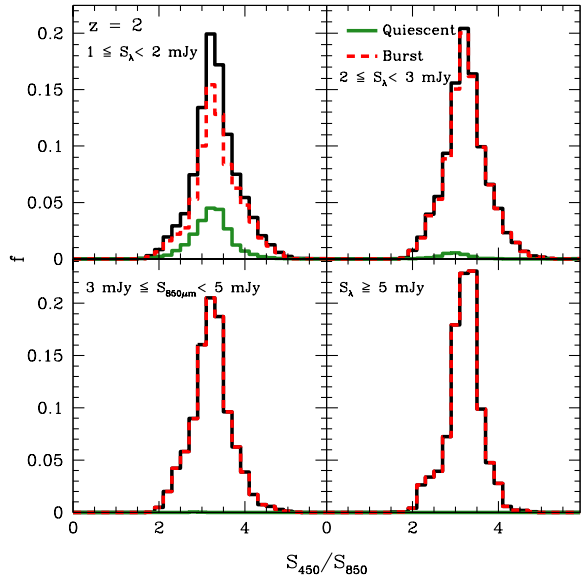


**Figure 12.** Distribution of the  $S_{450\mu\text{m}}/S_{850\mu\text{m}}$  flux ratio or colour for SMGs at  $z = 2$ , as a function of  $850\mu\text{m}$  flux density. The solid red and dashed orange histograms show the distribution for quiescent and starburst galaxies, respectively, while the black line displays the combined distribution. Quiescent galaxies only make a significant contribution at the faintest fluxes (top left). The distributions are normalized to integrate to unity.

full sample. Currently, there are no observational determinations of this relation at the redshifts of interest for SMGs.

### 4.3 Dependence of clustering on sub-mm colour

Before studying the dependence of the correlation length,  $r_0$ , on sub-mm colour, as given by the  $S_{450\mu\text{m}}/S_{850\mu\text{m}}$  flux ratio, it is informative to first plot the colour distribution itself, which we show in Fig. 12. Here, we separate galaxies into bins of  $S_{850\mu\text{m}}$  flux and discriminate between quiescent and starburst galaxies. In our model, the  $S_{450\mu\text{m}}/S_{850\mu\text{m}}$  colour distribution of  $\lambda = 850\mu\text{m}$  selected galaxies peaks around  $\approx 3.2$ . Furthermore, we find that the mode and shape of the colour distribution does not change significantly with  $S_{850\mu\text{m}}$  flux, i.e. the colour–luminosity relation of sub-mm galaxies with  $S_{850\mu\text{m}} \geq 1$  mJy is roughly constant. Also, there is very little difference between the colour distribution of starburst and quiescent galaxies (note, however, that, at lower fluxes, the fraction of sub-mm galaxies which are forming stars quiescently increases).

The observed distribution of  $450\mu\text{m}/850\mu\text{m}$  colours of SMGs has not yet been accurately measured, but the  $350\mu\text{m}/850\mu\text{m}$  colours of SMGs in the same model were investigated by Swinbank et al. (2008), who found the predicted colours to be in agreement with observed values. They also found that the median  $350\mu\text{m}/850\mu\text{m}$  colour of model SMGs could be fit by a modified blackbody spectrum  $L_\nu \propto B_\nu(T) \nu^\beta$ , with  $\beta = 1.5$  and an effective dust temperature of  $T = 32$  K. This modified blackbody implies a colour  $S_{450\mu\text{m}}/S_{850\mu\text{m}} \approx 3.5$  for SMGs at  $z = 2$ , which agrees well with the distribution plotted in Fig. 13.

In Fig. 13 we plot the correlation length,  $r_0$ , as a func-

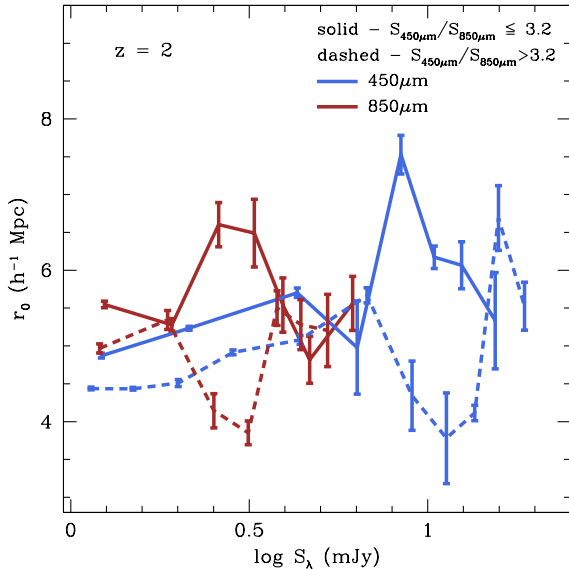


**Figure 13.** Dependence of the correlation length,  $r_0$ , on  $S_{450\mu\text{m}}/S_{850\mu\text{m}}$  colour for galaxies at  $z = 2$ . SMGs selected by their emission at  $\lambda = 850\mu\text{m}$  are represented by the red line, while the predictions for galaxies selected at  $\lambda = 450\mu\text{m}$  are plotted in blue. Solid and dashed lines show the correlation length for galaxies split by sub-mm colour,  $S_{450\mu\text{m}}/S_{850\mu\text{m}}$ , as indicated by the key.

tion sub-mm flux for two samples split at a sub-mm colour of  $S_{450\mu\text{m}}/S_{850\mu\text{m}} = 3.2$ . The dependence of  $r_0$  on luminosity is similar to that shown in Fig. 9. The figure also hints that redder galaxies, i.e. those with  $S_{450\mu\text{m}}/S_{850\mu\text{m}} \leq 3.2$ , are more clustered than bluer galaxies with  $S_{450\mu\text{m}}/S_{850\mu\text{m}} \geq 3.2$  (for both  $\lambda = 850\mu\text{m}$  and  $\lambda = 450\mu\text{m}$  selected galaxies). For example, for  $S_{850\mu\text{m}} \approx 3$  mJy galaxies,  $r_0$  can differ by a factor of  $\approx 1.6$  between the red and blue samples.

Having plotted the colour distributions of starburst and quiescent galaxies and the relation between  $r_0$  and sub-mm colour, it is useful to study the clustering of quiescent and starburst galaxies separately. As mentioned in connection with Fig. 12, quiescent galaxies only make a significant contribution at lower fluxes,  $S_{850\mu\text{m}} \leq 2$  mJy. In Fig. 14, we plot the two-point correlation function in real-space of sub-mm galaxies selected by  $S_{850\mu\text{m}} \geq 1$  mJy at  $z = 2$ . We also plot the correlation functions of quiescent and starburst galaxies separately. Fig. 13 reveals that, in our model, quiescent galaxies are more clustered than burst galaxies of similar sub-mm luminosities, on all scales. This is mostly due to the fact that quiescent SMGs are more massive than burst SMGs, due to both the top-heavy IMF and shorter star formation timescale in bursts. We compute  $r_0 = 5.2 h^{-1}$  Mpc for burst galaxies with  $S_{850\mu\text{m}} \geq 1$  mJy, and  $r_0 = 7.2 h^{-1}$  Mpc for quiescent galaxies brighter than the same flux limit.

## 5 DISCUSSION AND CONCLUSIONS

In this paper we have applied the technique introduced by Almeida et al. (2010), based on artificial neural networks, to predict the spatial and angular clustering of sub-mm selected galaxies (SMGs) in a  $\Lambda$ CDM universe. The ANN al-

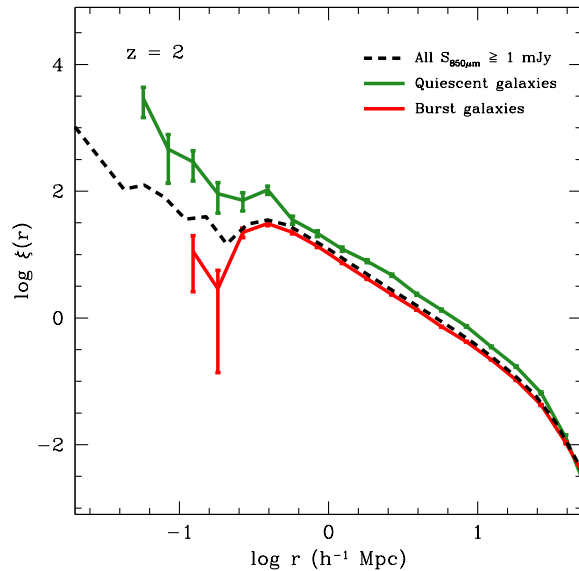


**Figure 14.** The real-space two-point correlation function of quiescent (red line) and starburst (orange) sub-mm galaxies, selected by  $S_{850\mu\text{m}} \geq 1$  mJy at  $z = 2$ . The dashed black line shows the correlation function for all galaxies with fluxes brighter than 1 mJy.

lows us to rapidly mimic the predictions of a hybrid code, made up of the GALFORM semi-analytical model of galaxy formation, which predicts the full star formation and merger histories of galaxies, and the GRASIL code, which computes the spectral energy distributions of galaxies self-consistently. This makes it possible for large N-body simulations of the hierarchical growth of structure in the dark matter to be populated with galaxies with full SED coverage from the UV through to the radio. The ANN technique requires as input a small set of galaxy properties predicted by GALFORM. We use the algorithm to populate the Millennium Simulation with  $\lambda = 850\mu\text{m}$  and  $\lambda = 450\mu\text{m}$  selected galaxies, with  $S_\lambda \geq 1$  mJy. The accuracy of the artificial neural network is notable: for SMGs at  $z = 2$ , we are able to reproduce the luminosity of  $\approx 95$  per cent of galaxies to within 10 per cent of the true values. The errors introduced by this technique in the determination of clustering properties are negligible.

We have presented predictions for the two-point spatial and angular correlation functions, for samples of galaxies selected at  $850\mu\text{m}$  and  $450\mu\text{m}$ . At  $z = 2$ , we predict a comoving correlation length of  $r_0 = 5.6 \pm 0.9 h^{-1}\text{Mpc}$  for galaxies with  $S_{850\mu\text{m}} \geq 5$  mJy and  $r_0 = 5.38 \pm 0.02 h^{-1}\text{Mpc}$  for fainter galaxies, brighter than 1 mJy. The former value is in good agreement with the indirect observational estimate by Blain et al. (2004) who found  $r_0 = 6.9 \pm 2.1 h^{-1}\text{Mpc}$  for a small sample of SMGs with  $S_{850\mu\text{m}} \sim 5$  mJy. Galaxies selected at  $\lambda = 450\mu\text{m}$  are less clustered than those identified at  $850\mu\text{m}$  galaxies, to the same flux limit.

Not surprisingly, the correlation length of sub-mm selected galaxies evolves with redshift: galaxies selected at higher redshifts display larger comoving correlation lengths, i.e. with increasing redshift they trace more overdense (and consequently, rarer) regions of the Universe. This behaviour is similar to that expected for the growth of structures in a

$\Lambda$ CDM universe, and further supports the idea that sub-mm galaxies are biased tracers of the underlying mass.

We have also studied the dependence of clustering on some properties of our sub-mm galaxies. Generally, we found a strong dependence of clustering on luminosity, with brighter galaxies displaying higher correlation lengths. We predict a tight correlation between halo mass and clustering scale, with sub-mm galaxies hosted by massive haloes being more clustered than those hosted by less massive ones. We find that the relation found for SMGs is not significantly different from the clustering of all haloes of the same mass. A similar behaviour is observed for the correlation between clustering and total stellar mass. We find that more massive sub-mm galaxies are more clustered than less massive one (in fact, massive galaxies are predominately found in more massive haloes – haloes with higher effective bias): in our model,  $r_0$  changes by a factor of  $\approx 2$  within the range  $\log M_* \approx [9.5, 10.5] h^{-1}M_\odot$ . The dependence of clustering on sub-mm colour,  $S_{450\mu\text{m}}/S_{850\mu\text{m}}$ , is not so clear. We find a weak positive correlation between  $r_0$  and colour, with redder galaxies being more strongly clustered. Finally, we predict that for galaxies selected to have  $S_{850\mu\text{m}} \geq 1$  mJy, quiescent galaxies are more clustered than those undergoing a burst of star formation.

It is important to note that current observational measurements of the clustering properties of sub-mm selected galaxies are limited due to poor statistics. At  $z \sim 2$ , estimations of the correlation function currently rely on samples with fewer than  $\sim 100$  galaxies. However, this picture will soon be improved. A more detailed comparison will soon be possible with the forthcoming instruments, such as the SCUBA-2, which will allow a much deeper and wider survey of the submillimetre population up to redshift 4 than current instruments. A more accurate determination of the clustering will, by then, impose serious constraints on the theories of galaxy formation and evolution.

## ACKNOWLEDGEMENTS

C. A. gratefully acknowledges support from the NSFC Research Fellowship for International Young Scientists, grant no 10950110319. This work was supported by the Chinese Academy of Sciences, grant no. 2009YB1, and by the Science and Technology Facilities Council rolling grant to the ICC.

## REFERENCES

- Alexander D. M., Bauer F. E., Brandt W. N., Hornschemeier A. E., Vignali C., Garmire G. P., Schneider D. P., Chartas G., Gallagher S. C., 2003, MNRAS, AJ, 125, 383
- Alexander D. M., Bauer F. E., Chapman S. C., Smail I., Blain A. W., Brandt W. N., Ivison R. J., 2005, ApJ, 632, 736
- Almeida C., Baugh C. M., Lacey C. G., 2007, MNRAS, 376, 1711
- Almeida C., Baugh C. M., Wake D. A., Lacey C. G., Benson A. J., Bower R. G., Pimbblet K., 2008, MNRAS, 386, 2145
- Almeida C., Baugh C. M., Lacey C. G., Frenk C. S., Granato G. L., Silva L., Bressan A., 2010, MNRAS, 402, 544
- Angulo R. E., Baugh C. M., Frenk C. S., Lacey C. G., 2008, MNRAS, 383, 755

- Angulo R. E., Lacey C. G., Baugh C. M., Frenk C. S., 2009, MNRAS, 399, 983
- Barger A. J., Cowie L. L., Sanders D. B., Fulton E., Taniguchi Y., Sato Y., Kawara K., Okuda, H., 1998, Nat, 394, 248
- Baugh C. M., Benson A. J., Cole S., Frenk C. S., Lacey C. G., 1999, MNRAS, 305, 21
- Baugh C. M., Lacey C. G., Frenk C. S., Granato G. L., Silva L., Bressan A., Benson A. J., Cole S., 2005, MNRAS, 356, 1191
- Baugh C. M., 2006, Rep. Prog. Phys., 69, 3101
- Benson A. J., Baugh C. M., Cole S., Frenk C. S., Lacey C. G., 2000, MNRAS, 316, 107
- Benson A. J., Bower R. G., Frenk C. S., Lacey C. G., Baugh C. M., Cole S., 2003, ApJ, 599, 38
- Benson A. J., 2010, Phys. Rep., in press, (arXiv:1006.5394)
- Berlind A. A., Weinberg D. H., 2002, ApJ, 575, 587
- Berlind A. A., et al., 2003, ApJ, 539, 1
- Biggs A. D., Ivison R. J., 2008, MNRAS, 385, 893
- Blain A. W., Smail I., Ivison R. J., Kneib J. -P., Frayer D. T., 2002, Phys. Rep., 369, 111
- Blain A. W., Chapman S. C., Smail I., Ivison R., 2004, ApJ, 611, 725
- Borys C., Smail I., Chapman S. C., Blain A. W., Alexander D. M., Ivison R. J., 2005, ApJ, 635, 853
- Bower R. G., Benson A. J., Malbon R., Helly J. C., Frenk C. S., Baugh C. M., Cole S., Lacey C. G., 2006, MNRAS, 370, 645
- Bressan A., Silva L., Granato G. L., 2002, A&A, 392, 377
- Brodwin M., et al., 2008, ApJ, 687, 65
- Bruzual G., Charlot S., 2003, MNRAS, 344, 1000
- Casey C. M., Chapman S. C., Muxlow T. W. B., Beswick R. J., Alexander D. M., Conzelmann C. J., 2009, MNRAS, 395, 1249
- Chapman et al., 2000, MNRAS, 319, 318
- Chapman S. C., Blain A. W., Smail I., 2005, ApJ, 622, 772
- Cole S., Lacey C. G., Baugh C. M., Frenk C. S., 2000, MNRAS, 319, 168
- Cooray A., Sheth R., 2002, Physics Reports, 372, 1
- Cooray A., et al., 2010, A&A, 518, 22
- Croton D. J., et al., 2006, MNRAS, 365, 11
- Dunne L., Eales S., Edmunds M., 2003, MNRAS, 341, 589
- Eke V. R., et al., 2004, MNRAS, 355, 769
- Elmegreen B. G., 2009, in *The Evolving ISM in the Milky Way and Nearby Galaxies*
- Engelbracht C. W., et al., 2006, ApJ, 642, 127
- Farrar D., et al., ApJ, 641, L17
- Ferrara A., Bianchi S., Cimatti A., Giovanardi C., 1999, ApJS, 123, 423
- Font A. S., et al., 2008, MNRAS, 389, 1619
- Gao L., Springel V., White S. D. M., 2005, MNRAS, 363, L66
- González J. E., Lacey C. G., Baugh C. M., Frenk C. S., Benson A. J., 2009, MNRAS, 397, 1254
- González J. E., Lacey C. G., Baugh C. M., Frenk C. S., 2010a, MNRAS, submitted
- González J. E., Lacey C. G., Baugh C. M., Frenk C. S., 2010b, MNRAS, submitted (arXiv:1006.0230)
- Gonzalez-Perez V., Baugh C. M., Lacey C. G., Almeida C., 2009, MNRAS, 398, 497
- Granato G. L., Lacey C. G., Silva L., Bressan A., Baugh C. M., Cole S., Frenk C. S., 2000, ApJ, 542, 710
- Guiderdoni B., Hivon E., Bouchet F. R., Maffei B., 1998, MNRAS, 295, 877
- Guo, et al., 2010, MNRAS, submitted
- Harker G., Cole S., Helly J., Frenk C., Jenkins A., 2006, MNRAS, 367, 1039
- Hainline L. J., Blain A. W., Smail I., Alexander D. M., Armus L., Chapman S. C., Ivison R. J., 2010, MNRAS, submitted (arXiv:1006.0238)
- Hughes D. H., Dunlop J. S., Rawlings S., 1997, MNRAS, 289, 766
- Ivison R. J., Smail I., Barger A. J., Kneib J. -P., Blain A. W., Owen F. N., Kerr T. H., Cowie L. L., 2000, MNRAS, 315, 209
- Jennings E., Baugh C. M., Pascoli S., 2010, MNRAS, submitted (arXiv:1003.4282)
- Kaiser N., 1987, MNRAS, 227, 1
- Kennicutt R. C., 1983, ApJ, 272, 54
- Kim H.-S., Baugh C. M., Cole S., Frenk C. S., Benson A. J., 2009, MNRAS, 400, 1527
- Kim H.-S., Baugh C. M., Benson A. J., Cole S., Frenk C. S., Lacey C. G., Power C., Schneider M., 2010, MNRAS, submitted (arXiv:1003.0008)
- Kroupa P., 2001, MNRAS, 322, 231
- Lacey C. G., Baugh C. M., Frenk C. S., Silva L., Granato G. L., Bressan A., 2008, MNRAS, 385, 1155
- Lacey C. G., Baugh C. M., Frenk C. S., Benson A. J., Orsi A., Silva L., Granato G. L., Bressan, A., 2010a, MNRAS, 405, 2
- Lacey C. G., Baugh C. M., Frenk C. S., Benson A. J., 2010b, MNRAS, submitted (arXiv:1004.3545)
- Lagos C. D. P., Cora S. A., Padilla N. D., 2008, MNRAS, 388, 587
- Landy S., Szalay A., 1993, ApJ, 412, 64
- Le Delliou M., Lacey C. G., Baugh C. M., Morris S. L., 2006, MNRAS, 365, 712
- Li A., Draine B. T., 2001, ApJ, 554, 778
- Li C., Kauffmann G., Jing Y. P., White S. D. M., Börner G., Cheng F. Z., 2006, MNRAS, 368, 21
- Limber D. N., 1953, ApJ, 117, 134
- Maddox S. J., et al., 2010, A&A, 518, 11
- Michalowski M. J., Hjorth J., Watson D., 2010, A&A, 514, 67
- Mo H. J., White S. D. M., 1996, MNRAS, 282, 347
- Meneux B., et al., 2008, A&A, 478, 299
- Nagashima, M., Lacey, C. G., Baugh, C. M., Frenk, C. S., & Cole, S. 2005, MNRAS, 358, 1247
- Nagashima M., Lacey C. G., Okamoto T., Baugh C. M., Frenk C. S., Cole S., 2005, MNRAS, 363, 31
- Norberg P., et al., 2001, MNRAS, 328, 64
- Orsi A., Lacey C. G., Baugh C. M., Infante L., 2008, MNRAS, 391, 1589
- Panuzzo P., Granato G. L., Buat V., Inoue A. K., Silva L., Iglesias-Páramo J., Bressan A., 2007, MNRAS, 375, 640
- Peebles P. J. E., 1980, *The large-scale structure of the Universe*, Princeton, N.J., Princeton University Press
- Percival W. J., Scott D., Peacock J. A., Dunlop J. S., 2003, MNRAS, 338, 31
- Pope et al., 2008, ApJ, 675, 1171
- Power C., Baugh C. M., Lacey C. G., 2010, MNRAS, 406, 43
- Riedmiller M., Braun H., 1993, Proc. of the IEEE Intl. Conf. on Neural Networks, 586
- Schurer A., Calura F., Silva L., Pipino A., Granato G. L., Matteucci F., Maiolino R., 2009, MNRAS, 394, 2001
- Scott S. E., et al., 2002, MNRAS, 331, 817
- Scott, S. E., Dunlop, J. S., & Serjeant, S. 2006, MNRAS, 370, 1057
- Seljak U., 2000, MNRAS, 318, 203
- Sheth R. K., Mo H. J., Tormen G., 2001, MNRAS, 323, 1
- Silva L., Granato G. L., Bressan A., Danese L., 1998, ApJ, 509, 103
- Silva L., Schurer A., Granato G. L., Almeida C., Baugh C. M., Frenk C. S., Lacey C. G., Paoletti L., Petrella A., Selvestrel D., 2010, MNRAS, submitted, (arXiv:1006.4637)
- Simon P., 2007, A&A, 473, 711
- Smail I., Ivison R. J., Blain A. W., 1997, ApJ, 490, L5
- Smail I., Ivison R. J., Blain A. W., Kneib J. -P., 2002, MNRAS, 331, 495
- Solomon P. M., Vanden Bout P. A., 2005, ARA&A, 43, 677
- Springel V., et al., 2005, Nature, 435, 629
- Swinbank A. M., et al., 2008, MNRAS, 391, 420
- Tacconi L. J., et al., 2006, ApJ, 640, 228

- van Kampen E., et al., 2005, MNRAS, 359, 469  
Vega O., Silva L., Panuzzo P., Bressan A., Granato G. L., Chavez M., 2005, MNRAS, 364, 1286  
Weiß A., et al., 2009, ApJ, 707, 1201  
Wilman R. J., Gerssen J., Bower R. G., Morris S. L., Bacon R., de Zeeuw P. T., Davies R. L., 2005, Nature, 436, 227  
Zehavi I., et al., 2005, ApJ, 621, 22